SAND2013-3038C
Proceedings of Proceedings of the ASME 2013 Fluids Engineering Summer Meeting FEDSM2013
July 7-11, 2013, Incline Village, Nevada, USA

FEDSM2013-16560

UNCERTAINTY QUANTIFICATION OF THE HYBRID METHOD FOR PARTICLE FIELD MEASUREMENT USING DIGITAL IN-LINE HOLOGRAPHY

Jian Gao and Jun Chen*
School of Mechanical Engineering
Purdue University
West Lafayette, Indiana 47907

Daniel R. Guildenbecher
Phillip L. Reu
Sandia National Laboratories
Albuquerque, New Mexico 87185

ABSTRACT

Digital in-line holography has been applied extensively to particle field measurement, where the particles can be the tracer particles for flow measurement, droplets in spray diagnostics, or aquatic microorganisms. The particle detection algorithm plays a key role in accurate detection of particle 3D locations and sizes. A hybrid method has recently been proposed for particle field measurement in digital in-line holography. It features automatic determination of the threshold for segmentation of the particle field and the capability to measure particles of arbitrary shapes. Using the hybrid method, the particle 3D location, size and shape information can be extracted. The uncertainty of the hybrid method is characterized using both synthetic and experimental holograms at different particle field conditions. The depth measurement uncertainty is within 2 times the particle diameter for a wide range of particle field conditions.

NOMENCLATURE

E_r	reconstructed complex amplitude
h	hologram
R	complex amplitude of reference wave
g	Rayleigh-Sommerfeld diffraction kernel
z_r	reconstruction distance
z_d	detected particle depth
k	wave number
λ	wavelength
M	number of pixels in horizontal direction
N	number of pixels in vertical direction
$\Delta\xi$	dimension of pixel in horizontal direction
$\Delta\eta$	dimension of pixel in vertical direction
A	reconstructed amplitude
I	reconstructed intensity
T	Tenengrad map
D_T	depth map
S_x	horizontal Sobel kernel
S_y	vertical Sobel kernel
S	quantified sharpness
D	particle diameter
w	particle width
h	particle height
F	Fresnel number
L	distance between hologram plane and particle field
σ	relative mean deviation
Δz_d	average displacement

INTRODUCTION

Digital in-line holography has been applied to measure particle fields where the particles can be tracer particles, drops, microorganisms, etc. In particular, it has been applied to flow visualization and measurement [1–3], spray diagnostics [4–6], mobility and behavior study of micro-organism [7, 8], study of atmospheric particles [9], and other subjects. The performance of digital holography for particle field measurement replies heavily on the accurate determination of 3D location of particles, especially the depthwise location. When the particle size and geometry are

*Corresponding author; junchen@purdue.edu

of primary interest, it is particularly important to determine the focus depth of a particle to accurately extract the size and shape of a specific particle. In addition to the hardware factors (e.g., pixel resolution of digital cameras) that affect the accuracy in locating a particle, the algorithms (methods) used to extract the depth can also have a remarkable influence on the uncertainty of measurement.

The methods to determine the depth of a particle in digital holography can be categorized into two categories. The first one includes methods that utilize the intensity (amplitude) pattern of the reconstructed particle image. It is assumed that when the in-line hologram of a particle is reconstructed at the particle's true depth, i.e., focal plane of the particle, the criterion for focus, which is based on the analysis of reconstructed intensity (amplitude) information, reaches its extreme [10–19]. The second category includes approaches that use the complex amplitude information of the reconstructed wave [20–22]. Though various methods are developed, they often suffer from several problems which prevent them from being applied to situations where measurement uncertainties are of primary concern. First of all, the measurement uncertainties are often characterized insufficiently, using both synthetically generated and experimentally acquired holograms. The results from synthetic holograms are considered an estimation of the achievable optimal accuracy of a method, due to the lack of, e.g., noises and imperfections of recording media that always present in experimental conditions. As a result, experimental holograms can be used to further investigate the influences of these factors on the accuracy of the method. Therefore, both numerical and experimental results are indispensable to systematically characterize the uncertainty of a algorithm. Secondly, the parameters of the particle field used for accuracy characterization are often far different from those of the particle field in real measurements. For example, the uncertainty obtained from detecting of a single particle is likely to be underestimated comparing to the uncertainty when the method is applied to a dense particle field. Thirdly, certain existing methods are only capable of measuring spherical particles, whereas in many practical applications the particles often have arbitrary shapes. Finally, manual input of threshold according to empirical values or knowledge about the particle field is often required to segment an image of multiple particles to detect particles individually.

Recently, a hybrid method [23], which features automatic determination of threshold for segmentation and capability to detect particles of arbitrary shapes, is proposed to overcome the aforementioned limitations of existing particle detection methods. In this paper, we characterize the uncertainty of this new method both numerically and experimentally. The paper is organized as follows. Digital in-line holography is first briefly introduced, followed by an elaboration on the implementation of the hybrid method. The measurement uncertainty of the hybrid method is quantified using both synthetic holograms and experimental holograms. Finally, conclusions are drawn on the depth determination accuracy of the hybrid method.

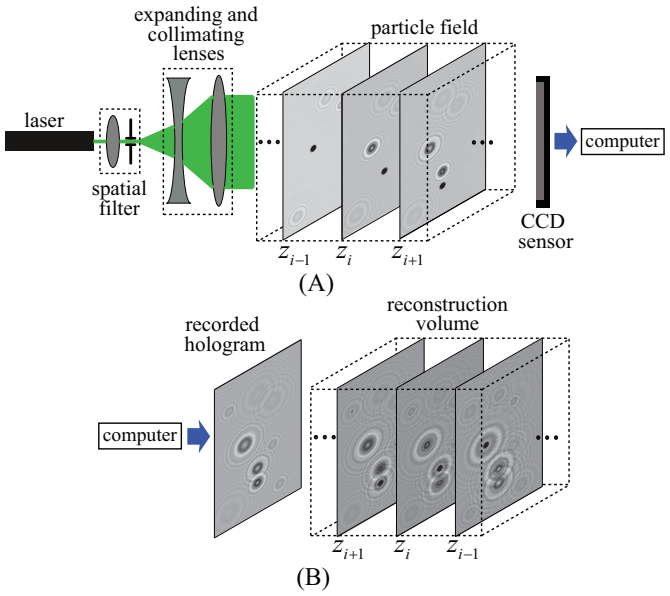

FIGURE 1. SCHEMATIC OF DIGITAL IN-LINE HOLOGRAPHY FOR PARTICLE FIELD DETECTION: (A) RECORDING AND (B) RECONSTRUCTION.

DIGITAL IN-LINE HOLOGRAPHY

Shown in Fig. 1(A) is a typical setup of digital in-line holography for measurement of a particle field. The laser beam is spatially filtered, expended and collimated before illuminating the particle field. The light diffracted and scattered by the particles is the object wave, and the undisturbed part of the same beam serves as the reference wave. The interference pattern (hologram) is recorded by the CCD sensor and stored in a computer as a digital image $h(m,n)$. In the reconstruction step, by varying the reconstruction distance z_r, particles at different planes of the reconstruction volume can be brought into focus in the reconstructed images, as shown in Fig. 1(B). The angular spectrum method is adopted to perform the numerical reconstruction, which can be expressed as [24]

$$E_r(x,y,z_r) = [h(\xi,\eta)R^*(\xi,\eta)] \otimes g(\xi,\eta,z_r), \tag{1}$$

where

$$g(\xi,\eta,z_r) = \frac{1}{j\lambda} \frac{\exp\left(jk\sqrt{\xi^2+\eta^2+z_r^2}\right)}{\sqrt{\xi^2+\eta^2+z_r^2}} \tag{2}$$

is the Rayleigh-Sommerfeld diffraction kernel. $E_r(x,y,z_r)$ is the complex amplitude reconstructed at z_r. (ξ,η) and (x,y) are coordinates in the hologram plane and reconstruction plane, respectively. $R(\xi,\eta)$ is the complex amplitude of the reference wave, * denotes complex conjugate, and $\otimes$ denotes convolution operation. λ and k are the wavelength and wave number, respectively. The discretized evaluation of Eqn. (1) in the Fourier domain can be expressed as

$$E_r(k,l,z_r) = \mathscr{F}^{-1}\left\{\mathscr{F}\{h(m,n)R^*(m,n)\}\exp\left(jkz_r\sqrt{1-\left(\frac{\lambda m}{M\Delta\xi}\right)^2-\left(\frac{\lambda n}{N\Delta\eta}\right)^2}\right)\right\}, \tag{3}$$

where $R(m,n)=1$, because the reference wave is a uniform plane wave. M and N are the number of pixels of the CCD sensor in the ξ and η directions, respectively, while $\Delta\xi$ and $\Delta\eta$ are dimensions of an individual pixel. $\mathscr{F}$ and $\mathscr{F}^{-1}$ denote fast Fourier transform and inverse fast Fourier transform, respectively. The reconstructed amplitude and intensity are

$$A(k,l,z_r) = |E_r(k,l,z_r)|, \tag{4}$$

and

$$I(k,l,z_r) = |E_r(k,l,z_r)|^2. \tag{5}$$

The reconstruction distance at which a particle is in focus is decided as the depth (z position) of the particle. The transverse position, particle size and shape can be determined from the focused image of the particle.

IMPLEMENTATION OF THE HYBRID METHOD

The hybrid method falls into the first category of particle detection method that uses the intensity or amplitude of the reconstructed particle image [23]. It relies on maximizing the edge sharpness of a particle image. Here, algorithms for particle detection, particle refinement and synthetic hologram generation are all coded using LabVIEW.

Detection of A Single Particle

The sharpness is quantified by calculation of the Tenengrad value across a particle image [25]. The Tenengrad map $T(k,l,z_r)$ at a reconstruction distance z_r can be obtained by

$$T(k,l,z_r) = [A(k,l,z_r)\otimes S_x]^2 + [A(k,l,z_r)\otimes S_y]^2, \tag{6}$$

where S_x and S_y are the horizontal and vertical Sobel kernels, respectively. The hologram is reconstructed at sequential planes in a reconstruction volume ($z_{\min}\le z_r\le z_{\max}$) with a depth interval, where $z_{\min}$ and $z_{\max}$ are determined such that the particles of interest are all enclosed in the reconstruction volume. During volume reconstruction, the maximum-Tenengrad map $T_{\max}$, its depth map D_T and minimum-intensity map $I_{\min}$ are obtained:

$$T_{\max}(k,l) = \max_{z_r}\left(T(k,l,z_r)\right) \tag{7}$$

$$D_T(k,l) = \arg\max_{z_r}\left(T(k,l,z_r)\right) \tag{8}$$

$$I_{\min}(k,l) = \min_{z_r}\left(I(k,l,z_r)\right). \tag{9}$$

This process is illustrated by Figs. 2(A)-(D).

A binary image of the particle is extracted by thresholding $I_{\min}$. In the hybrid method, an optimal threshold is decided automatically. A thresholding operator $\mathscr{T}_t\{\}$ is defined, which outputs a binary image at threshold t. An edge detection operator $\mathscr{E}\{\}$ is applied on the binary image, and yields the edges of the segments in the binary image. Example results of these two operations are shown in Figs. 2(E) and (F). The sharpness of the edge pixels at threshold t can be quantified by applying a sharpness operator $S(t)$:

$$\mathrm{S}(t) = \frac{\sum_{k,l}\left(\mathscr{E}\{\mathscr{T}_t\{I_{\min}\}\}\cdot T_{\max}\right)}{\sum_{k,l}\mathscr{E}\{\mathscr{T}_t\{I_{\min}\}\}}, \tag{10}$$

where $\cdot$ denotes pointwise multiplication. An optimal threshold for $I_{\min}$ occurs when $S(t)$ reaches its maximum, which is also when the obtained binary image best describes the particle, as shown in Figs. 2(G) and (H). Therefore, the optimal threshold can be written as

$$t_{\text{opt}} = \arg\max_{t}\left(S(t)\right). \tag{11}$$

Since the edge sharpness of a reconstructed particle image reaches its maximum near the focus depth, the average depth of the determined edge pixels is taken as the detected depth z_d of the particle

$$z_d = \frac{\sum_{k,l}\left(\mathscr{E}\{\mathscr{T}_{t_{\text{opt}}}\{I_{\min}\}\}\cdot D_T\right)}{\sum_{k,l}\mathscr{E}\{\mathscr{T}_{t_{\text{opt}}}\{I_{\min}\}\}}. \tag{12}$$

Afterwards, the particle size, shape and transverse position can be determined from the binary image $\mathscr{T}_{t_{\text{opt}}}\{I_{\min}\}$. The particle depth is determined as z_d.

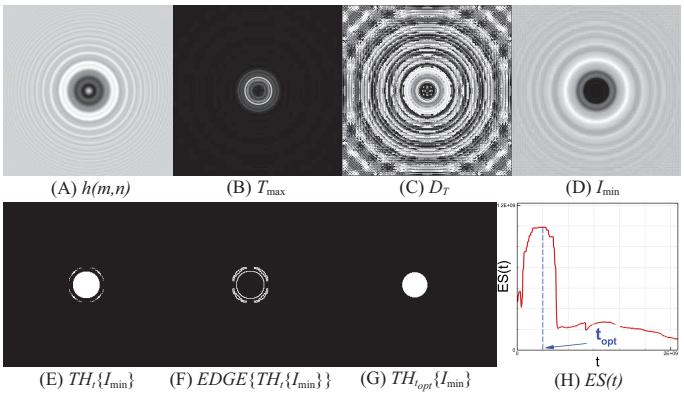

FIGURE 2. ILLUSTRATION OF DETECTION OF A SINGLE PARTICLE BY THE HYBRID METHOD

Detection of A Particle Field

In practical applications, the object of interest is a field of multiple particles. Individual particles in the particle field need to be identified during the application of a particle detection method. Consequently, the discrimination of particles from the background also influences the detection. Different approaches have been developed to segment a particle field to obtain the local windows that encloses individual particles. However, most of them require manual input of the thresholds for segmentation, which are decided based on empirical results. The empirical results are only applicable to certain experimental conditions, and thus their effectiveness degrades significantly as experimental conditions change.

First, the auto-selection of thresholds described in the previous section is applied globally to find an optimal threshold $t_{\text{opt,seg}}$ for segmenting the particles. The automated selection of the threshold eliminates the need of manual input. Subsequently, local windows are determined according to the (x, y) position and size of individual segments. Shown in Figs. 3(A)-(C) are a sample (synthetic) hologram of a particle field and the corresponding T_{max} and I_{min} obtained from volume reconstruction. The profile of the global sharpness, according to which the optimal threshold is found for segmentation, is shown in Fig. 3(D). The segments after thresholding using $t_{\text{opt,seg}}$ is shown in Fig. 3(E). Next, the automated routine is performed in the local window to determine the 3D position, size and shape information of the particle enclosed. The size of the local window is typically 2-3 times that of the corresponding segment. Finally, after each detected segment is processed, the information of the whole particle field is extracted.

Refinement of Detected Particles

Due to the limited size of the imaging sensor, the particles near the boarders of the detection volume lose part of their fringes in the hologram, leading to distorted reconstructed particle images with less sharp edges, as shown by the circled particle in Figs. 3(A) and (B). Accordingly, the particles near the boarder tend to have bigger measurement errors. To refine the detected particles, such particles can be removed from the group of detected particles. A minimum distance to the boarders of a hologram can be set based on different recording conditions (recording distance, particle size and etc.).

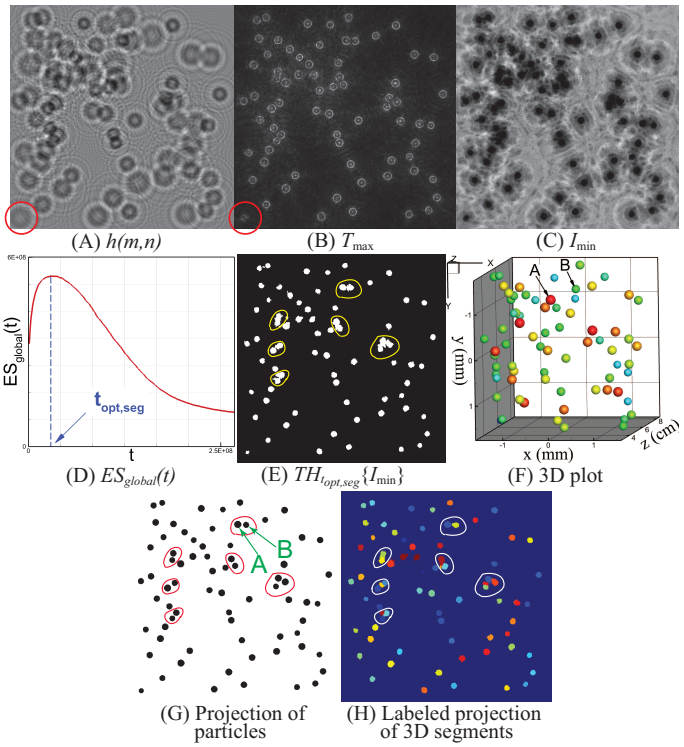

FIGURE 3. ILLUSTRATION OF SEGMENTATION OF A PARTICLE FIELD BY THE HYBRID METHOD AND REFINEMENT OF DETECTED PARTICLES

The measurement of transversely adjoining particles also tends to yield bigger errors. Figure. 3(F) shows a 3D plot of the particle field, of which the hologram in Fig. 3(A) is taken. Though particle A and particle B (indicated in the figure) are separated far from each other in the z (depth) direction, they are close in the (x, y) direction (transverse distance smaller than one particle diameter), as can be seen in Fig. 3(G), which is a projection image of the particle field along the depthwise direction. It is difficult to separate such particles in two-dimensional (2D) segmentation by the hybrid method, as shown in Fig. 3(E), where false segments that consists of more than one particle are detected. One can see that the circled false segments occur where the particles are close to one another in the transverse direction. The false segments not only leads to inaccurate depth measurement but also erroneous size measurement. In order to recognize the false segments, the hologram is volumetrically reconstructed,

during which 3D segmentation is conducted. The reconstructed intensity image is thresholded at each reconstruction distance z_r, and the 3D segments is formed by attaching the 2D segments obtained at each z_r according to their 3D connectivity. Since the particle field information is initially extracted by the hybrid method, the intensity threshold used in 3D segmentation can be determined as the median intensity of all of the particle images reconstructed at detected depths. Further, a limit on the cross-section area of the 3D segments can be chosen according to detected particle size information. Upon completion of the 3D segmentation, detected 3D segments are cast to the transverse plane with different labels, as shown in Fig. 3(H). Comparison between Figs. 3(E) and (H) shows that each false segment circled covers more than one label. In contrast, each correct segment that encloses only one particle corresponds to only one label. Accordingly, the false segments can be differentiated from correct segments by counting the number of corresponding labels. In the present study, the particles detected from false segments are eliminated directly from the group of detected particles. Further development of the algorithm is expected to separate the particles in false segments.

UNCERTAINTY QUANTIFICATION BY SYNTHETIC HOLOGRAMS

In digital in-line holography, the particle hologram records the interference pattern between the light scattered by the particle and the reference light. The interference pattern can be approximated by the diffraction pattern from an opaque mask corresponding to the cross-section of the particle. For particles of arbitrary shapes, Eqn. (3) can be used to simulate the holograms by substituting the mask function for $h(m,n)$. Particularly, to reduce the noise from space domain aliasing, a hologram of intended size are cropped from a hologram of bigger size, e.g., 1024×1024 cropped from 4096×4096. Holograms of spherical and rectangular particles can be simulated based on the analytical expression for Fresnel diffraction from circular and rectangular masks [23]. The intensity of the simulated hologram is scaled to 60% of the full scale of 14 bit, and is then added random noise of peak value 0.6% of the full scale. To characterize the uncertainties, the particle information extracted by the hybrid method is compared with the exact particle information, which is predetermined in the creation of synthetic holograms.

Detection Error for A Single Particle

Holograms of single particles of different shapes are simulated. The shapes include circle, rectangle, equilateral triangle, equilateral trapezoid, ellipse and "double-egg". The size of a particle is characterized by its diameter. For non-spherical particles, the diameter is the diameter of a disk with the same area as the particle. The particles are of diameter $D_0 = 35$, 50, 100, 150, 200, 250, 300, 400, 450 and 500 μm. Each of them is located at $z_0 = 0.05$, 0.10, 0.15, 0.20, 0.25, 0.30, 0.35 and 0.40 m from the hologram plane. A hologram is generated for each particle at each distance. Accordingly, for each type of particle, a total of 88 holograms are generated. The size of the hologram is 1024×1024 with 7.4×7.4 μm^2 pixels. The wavelength is 532 nm. The particle information determined by the hybrid method includes 3D coordinate (x_d, y_d, z_d), diameter D_d, width w_d and height h_d, which are then compared with the actual parameters to determine the relative errors.

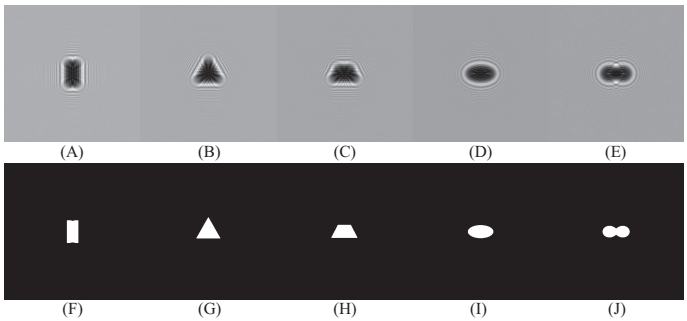

FIGURE 4. SAMPLE HOLOGRAMS OF NON-SPHERICAL PARTICLES (A)-(E) AND BINARY IMAGES EXTRACTED BY THE HYBRID METHOD (F)-(J).

The hybrid method is able to detect particles of arbitrary shapes, as shown in Fig. 4. The holograms and binary images shown are of size 512×512, cropped from the original size. The relative errors of particle parameters are plotted against the Fresnel number $F = D_0^2(4\lambda z_0)^{-1}$, as shown in Fig. 5. The Fresnel number is a non-dimensional parameter, which combines the particle size and distance information. Subscript "d" and "0 " denote determined value and actual value, respectively. The accuracy in transverse position measurement is on the order of 0.1 pixel size, except for certain shapes at very small Fresnel numbers, as shown in Figs. 5(A) and (B). The relative depth (z) error is with respective to the particle diameter, as shown in Fig. 5(C). The overall depth error is smaller than twice the particle diameter. When $F > 0.4$, the depth error is within the particle diameter. The shape parameters (diameter, width and height) can be measured with an overall relative error of 10%, as shown in Figs. 5(D)-(F). The tendency that the error grows as the Fresnel number decreases is observed. This may result from the loss of numerical aperture at smaller Fresnel numbers, and thus less orders of diffraction fringes can be recorded resulting in inaccurate determination of the edges of the particles by the hybrid method.

Detection Error for A Particle Field

Holograms of particle fields are simulated using Eqn. (3). The synthetic particle field has a dimension of 7.6 $mm \times$ 7.6 $mm \times 5$ cm, where 5 cm is the dimension in the depthwise

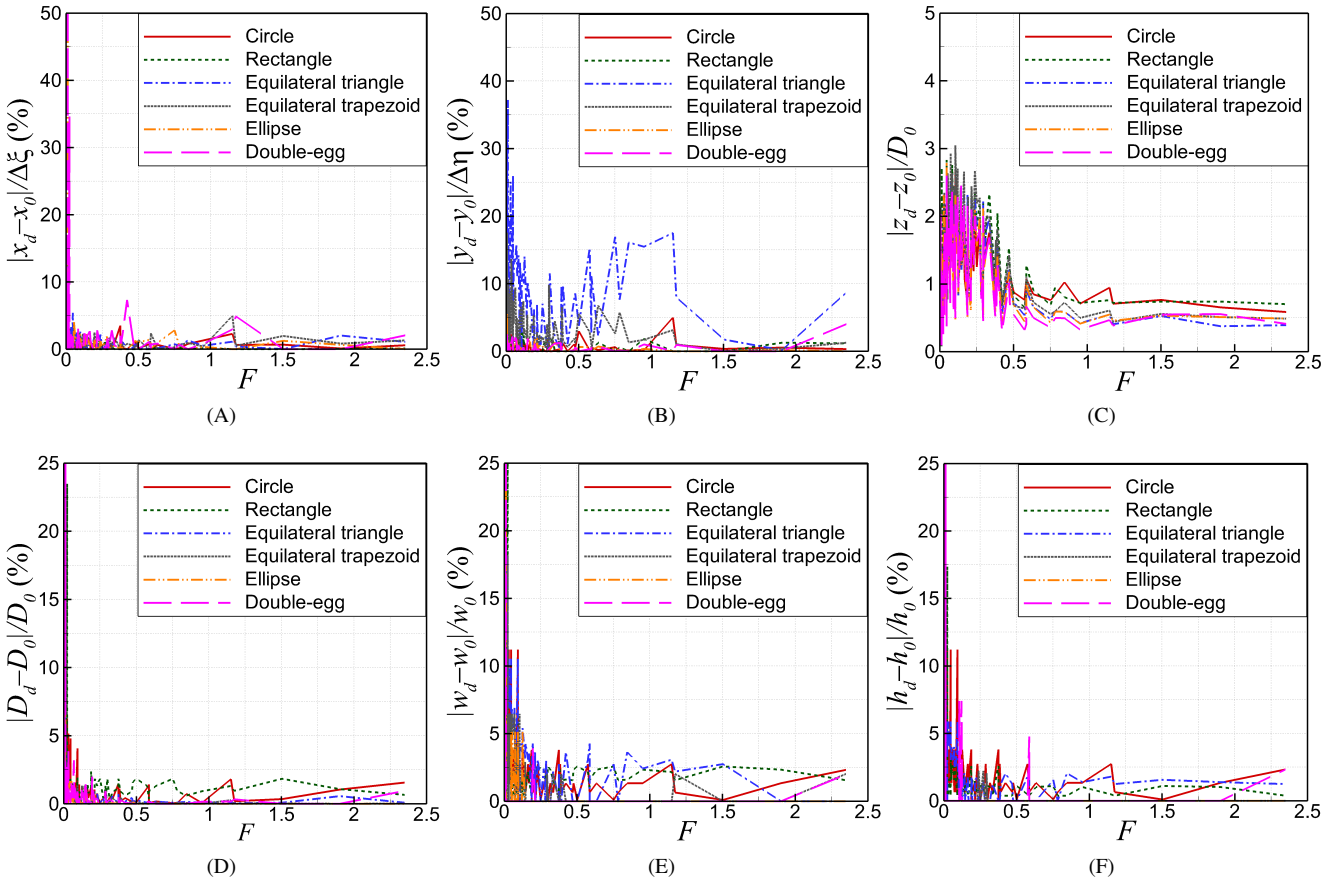

FIGURE 5. DETECTION ERRORS OF 3D LOCATION (A)-(C) AND SHAPE PARAMETERS (D)-(F).

direction. The particles are randomly distributed in the volume, and are separated transversely far from each other. Therefore, the effects of adjoining particles on accuracy are eliminated. Spherical particles of two kinds of diameter distribution are used in the simulation. The diameter of the bigger particle is normally distributed with mean diameter $D_{avg} = 100\ \mu m$, standard deviation 10 μm, and that of the smaller particle is also normally distributed with mean diameter 50 μm, standard deviation 10 μm. For each kind of particles, holograms are simulated at different particle number densities and distances from the hologram plane. ρ_N is the particle number density (number of particles over a unit area of the cross-section of the particle volume). L is the distance from the center of the particle volume to the hologram plane. The particle field is located at $L = 0.085\ m$ and $L = 0.145\ m$. The average Fresnel number $\bar{F}$ is evaluated by $D_{avg}^2(4\lambda L)^{-1}$. The holograms are processed by the hybrid method, and the depth of each detected particle is compared with the actual particle depth. The depth measurement accuracy is characterized by the cumulative distribution function (CDF) of the relative error. The resultant CDFs are shown in Fig. 6. The depth error increases at smaller Fresnel number, which coincide with the results in the detection of a single particle. The influence of particle number density on the accuracy is also seen that the measurement of a denser particle field tend to give higher errors. In general, 90% of the detected particles have a relative depth error less than 2, which also agrees with the previous results.

The size distribution of the particle field is also measured by the hybrid method, as shown in Fig. 7. Particles detected at different conditions are combined to generate the number probability density function (PDF) of the particle diameter. The detected profiles coincide qualitatively with the actual distribution profile. The sizes of particles can be determined more accurately at larger Fresnel number.

UNCERTAINTY QUANTIFICATION BY EXPERIMENTAL HOLOGRAMS

The uncertainty of the hybrid method is further characterized using experimental holograms. Holograms are taken of planar particle fields and 3D particle fields.

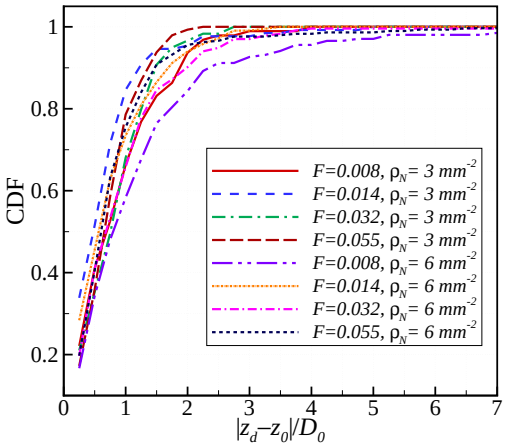

FIGURE 6. CDF OF RELATIVE DEPTH ERROR IN DETECTION OF PARTICLE FIELDS

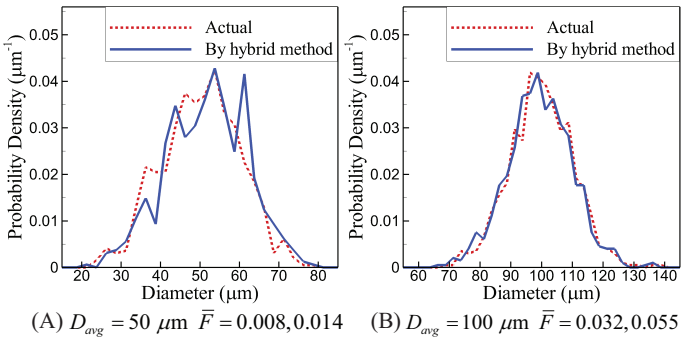

FIGURE 7. NUMBER PDF OF THE DIAMETER OF DETECTED PARTICLES

Detection of A Planar Particle Field

The planar particle field is created by putting SiO_2 (silicon dioxide) particles on a piece of plane glass. The surface of the glass, where the particles are placed, is normal to the depthwise direction. The glass is fixed on a translation stage, so that the particle field can be translated to different depth positions. The expanded and collimated beam from a He-Ne laser (wavelength 632.8 *nm*) is used to illuminate the particle field, and the hologram is recorded by a CCD camera with 2048×2048 7.4×7.4 μm^2 pixels (PCO2000). Only a 1500×700 part of the original hologram is processed. Shown in Fig. 8 are a part of the hologram (A), reconstructed intensity image at the average depth of all particles (B), corresponding 2D segments of particles determined by the hybrid method (C) and measured depth distribution of the particles (D). The arbitrary shapes of the particles are extracted accurately and represented by the 2D segments. The particles are distributed on a plane surface with several measurement outliers. The mean deviation from the average depth can be

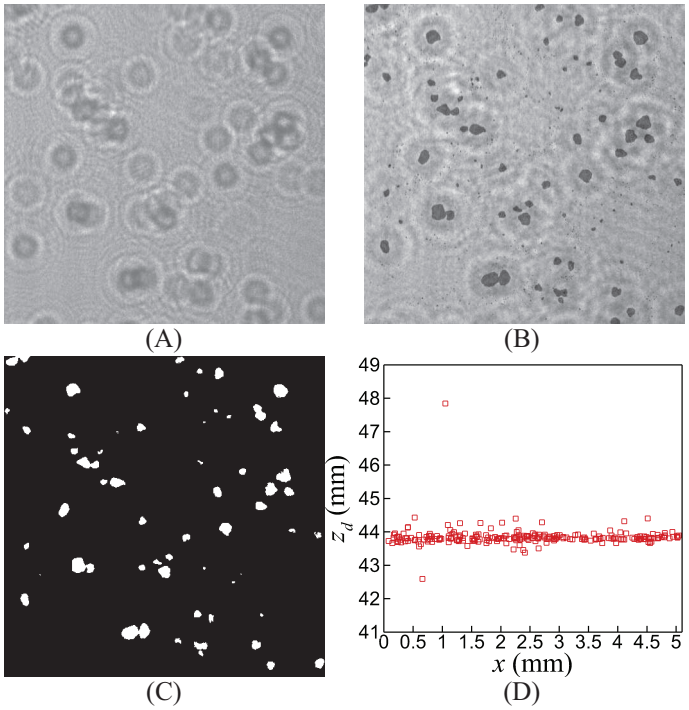

FIGURE 8. SAMPLE HOLOGRAM OF A PLANAR PARTICLE FIELD (A), EXAMPLE RECONSTRUCTION (B), CORRESPONDING BINARY IMAGE EXTRACTED (C) AND DEPTH DISTRIBUTION OF DETECTED PARTICLES (D).

expressed by

$$\delta = \frac{1}{K}\sum_{i}^{K}|z_{d,i} - z_{avg}|. \tag{13}$$

K is the number of detected particles. $z_{d,i}$ is the measured depth of an individual particle, and $z_{avg} = \sum z_{d,i}/K$ is the detected average depth. δ is found to be 115 μm, which is 1.4 times the detected average particle diameter D_{avg}.

The glass is translated to a sequence of depthwise positions, and the corresponding holograms are recorded and then processed by the hybrid method. From each hologram, the particle field information can be extracted, and an individual particle can be paired with its counterpart at neighbor depthwise position. Therefore, a displacement can be determined from each pair of particles, and the average displacement of all pairs of particles is taken as the measured displacement Δz_d of the glass, which can be determined by

$$\Delta z_d = \frac{1}{K}\sum_{i}^{K}\Delta z_{d,i}. \tag{14}$$

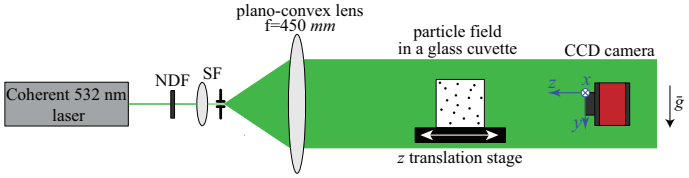

FIGURE 9. EXPERIMENTAL SETUP USED TO CAPTURE HOLOGRAMS OF A 3D PARTICLE FIELD. NDF: NEUTRAL DENSITY FILTER, SF: SPATIAL FILTER.

The relative mean deviation from the average displacement is used to quantify the uncertainty of depth measurement, which can be expressed as

$$\sigma = \frac{\sum_i^K |\Delta z_{d,i} - \Delta z_d|/K}{D_{avg}}. \tag{15}$$

Holograms of particle fields of different conditions are processed, and the results are shown in Tab. 1. The uncertainty is about one particle diameter, which is consistent with results obtained from synthetic holograms. The performance of the hybrid method is stable at different particle field conditions.

Detection of A 3D Particle Field

Holograms are also taken from 3D particle fields. The experimental setup used to capture the hologram is shown in Fig. 9. The particles are dispersed in a cubic cuvette with good optical transparency filled with silicone oil. Due to the high viscosity (10000 cSt) of the oil, the particles are assumed to be still in the volume. The inner dimension of the cuvette is the dimension of the particle field, which is 5 $cm \times 5$ $cm \times 5$ cm. Two kinds of polystyrene particles are mixed in the oil. One has mean diameter 115 μm, and the other has 550 μm mean diameter. The number density of the smaller particle is 4.9 mm^{-2}, and that of the bigger particle is 0.1 mm^{-2}. Therefore, the smaller particle dominates in the particle mixture. The size of the hologram is 1024×1024 with 7.4×7.4 μm^2 pixels. Similar to the planar particle field, the 3D particle field is translated to a sequence of depthwise positions. The hybrid method is applied to the holograms taken at different positions, and the detected particles are paired with their counterparts in consecutive frames. Due to the high number density of the 3D particle field, transversely close particles are a major contribution to the uncertainty. Therefore, the particle refinement procedure using 3D segmentation is used to eliminate the transverse-adjoining particles to improve the accuracy. The processing results before and after the refinement are shown in Tab. 2. The refinement results in significant reduction of uncertainty and more accurate determination of Δz_d. The uncertainty increases to about 3 times particle diameter, and at smaller Fresnel number, the relative uncertainty increases to 5. The degradation of the hybrid method is mainly due to the high number density of the 3D particle field. In reconstruction, the focused image of a particle is affected severely by the out-of-focus images of other particles in a dense particle field, leading to inaccurate sharpness quantification of the edge of the particle.

CONCLUSIONS

The hybrid method, which is based on maximizing the edge sharpness of the reconstructed particle image, has been proposed as a particle detection routine for digital in-line holography. The size, shape and 3D location information can be extracted for each particle in the volume. The method has the capability to segment a particle field automatically without the need to manually input the threshold for segmentation. In addition, the developed particle refinement approach is an effective way to improve the accuracy when the hybrid method is applied to a dense 3D particle field.

To characterize and quantify the uncertainty of measurements, the hybrid method is tested using both synthetic holograms and experimental holograms. The performance of the hybrid method is stable for particles of different particle shapes, sizes and distances. It is less sensitive to the noise due to diffraction from multiple particles, and thus it is robust when applied to particle field detection at moderate particle number density. For a wide range of experimental conditions, the uncertainty in depth measurement is estimated to be less than twice the particle diameter with a high certainty.

ACKNOWLEDGMENT

Sandia National Laboratories is a multiprogram laboratory operated by Sandia Corporation, a Lockheed Martin Company, for the United States Department of Energy's National Nuclear Security Administration under contract No. DE-AC04-94AL85000.

REFERENCES

[1] Meng, H., Pan, G., Pu, Y., and Woodward, S. H., 2004. "Holographic particle image velocimetry: from film to digital recording". *Meas. Sci. Technol.,* ***15***(4), p. 673.

[2] Sheng, J., Malkiel, E., and Katz, J., 2008. "Using digital holographic microscopy for simultaneous measurements of 3D near wall velocity and wall shear stress in a turbulent boundary layer". *Exp. Fluids,* ***45***, pp. 1023–1035.

[3] Chareyron, D., Mari, J. L., Fournier, C., Gire, J., Grosjean, N., Denis, L., Lance, M., and Ms, L., 2012. "Testing an in-line digital holography inverse method for the lagrangian tracking of evaporating droplets in homogeneous nearly isotropic turbulence". *New J. Phys.,* ***14***(4), p. 043039.

TABLE 1. DISPLACEMENT MEASUREMENT OF A PLANAR PARTICLE FIELD

Particle Field Parameters	Detected Displacement	Actual Displacement (μm)									
		127	127	127	127	127	635	635	635	635	635
$\bar{F} = 0.065$, $D_{avg} = 85\ \mu m$, $N_p = 4.0\ mm^{-2}$	Δz_d (μm)	125	126	134	127	153	619	653	628	632	636
	σ	0.8	0.9	0.8	0.8	1.2	1.4	1.0	1.2	1.1	1.1
$\bar{F} = 0.018$, $D_{avg} = 81\ \mu m$, $N_p = 1.6\ mm^{-2}$	Δz_d (μm)	121	145	129	120	130	620	638	642	679	659
	σ	0.9	0.7	0.9	1.0	1.1	1.2	1.3	1.3	1.3	1.3

TABLE 2. DISPLACEMENT MEASUREMENT OF A 3D PARTICLE FIELD

Particle Field Parameters	Post-processing		Actual Displacement (μm)				
			0	2000	0	2000	0
$\bar{F} = 0.078$, $D_{avg} = 122\ \mu m$	With Refinement	Δz_d (μm)	-134	2197	19	2024	-6
		σ	2.6	4.2	0.6	1.5	1.0
	Without Refinement	Δz_d (μm)	-33	2141	32	2414	219
		σ	5.5	5.8	3.4	9.0	3.9
$\bar{F} = 0.026$, $D_{avg} = 107\ \mu m$	With Refinement	Δz_d (μm)	37	1954	107	1956	67
		σ	4.0	5.5	3.4	4.1	3.2
	Without Refinement	Δz_d (μm)	278	2019	-191	2328	-77
		σ	8.2	10.5	7.4	10.8	7.0

[4] Lee, J., Sallam, K. A., Lin, K. C., and Carter, C. D., 2009. "Spray structure in near-injector region of aerated jet in subsonic crossflow". *J. Propul. Power,* ***25***, pp. 258–266.

[5] Lü, Q., Chen, Y., Yuan, R., Ge, B., Gao, Y., and Zhang, Y., 2009. "Trajectory and velocity measurement of a particle in spray by digital holography". *Appl. Opt.,* ***48***(36), pp. 7000–7007.

[6] Yang, Y., and seon Kang, B., 2011. "Digital particle holographic system for measurements of spray field characteristics". *Opt. Laser Eng.,* ***49***(11), pp. 1254 – 1263.

[7] Sheng, J., Malkiel, E., Katz, J., Adolf, J., Belas, R., and Place, A. R., 2007. "Digital holographic microscopy reveals prey-induced changes in swimming behavior of predatory dinoflagellates". *PNAS,* ***104***(44), pp. 17512–17517.

[8] Lee, S. J., Seo, K. W., Choi, Y. S., and Sohn, M. H., 2011. "Three-dimensional motion measurements of free-swimming microorganisms using digital holographic microscopy". *Meas. Sci. Technol.,* ***22***(6), p. 064004.

[9] Fugal, J. P., Shaw, R. A., Saw, E. W., and Sergeyev, A. V., 2004. "Airborne digital holographic system for cloud particle measurements". *Appl. Opt.,* ***43***(32), pp. 5987–5995.

[10] Sheng, J., Malkiel, E., and Katz, J., 2006. "Digital holographic microscope for measuring three-dimensional particle distributions and motions". *Appl. Opt.,* ***45***(16), pp. 3893–3901.

[11] Ilchenko, V., Lex, T., and Sattelmayer, T. "Depth position detection of the particles in digital holographic particle image velocimetry (DHPIV)". *Proc. SPIE,* ***5851***(123).

[12] Palero, V., Arroyo, M., and Soria, J., 2007. "Digital holography for micro-droplet diagnostics". *Exp. Fluids,* ***43***, pp. 185–195.

[13] Soulez, F., Denis, L., Fournier, C., Éric Thiébaut, and Goepfert, C., 2007. "Inverse-problem approach for particle digital holography: accurate location based on local optimization". *J. Opt. Soc. Am. A,* ***24***(4), pp. 1164–1171.

[14] Yang, Y., seon Kang, B., and jun Choo, Y., 2008. "Application of the correlation coefficient method for determination of the focal plane to digital particle holography". *Appl. Opt.,* ***47***(6), pp. 817–824.

[15] Fugal, J. P., Schulz, T. J., and Shaw, R. A., 2009. "Practical methods for automated reconstruction and characterization of particles in digital in-line holograms". *Meas. Sci. Technol.,* ***20***(7), p. 075501.

[16] Choi, Y.-S., and Lee, S.-J., 2009. "Three-dimensional volumetric measurement of red blood cell motion using digital holographic microscopy". *Appl. Opt.,* ***48***(16), pp. 2983–2990.

[17] Tian, L., Loomis, N., Domínguez-Caballero, J. A., and Barbastathis, G., 2010. "Quantitative measurement of size and three-dimensional position of fast-moving bubbles in air-water mixture flows using digital holography". *Appl. Opt.,* ***49***(9), pp. 1549–1554.

[18] Wu, Y., Wu, X., Wang, Z., Chen, L., and Cen, K., 2011. "Coal powder measurement by digital holography with expanded measurement area". *Appl. Opt.,* ***50***(34), pp. H22–H29.

[19] Yang, Y., Li, G., Tang, L., and Huang, L., 2012. "Integrated gray-level gradient method applied for the extraction of three-dimensional velocity fields of sprays in in-line digital holography". *Appl. Opt.,* ***51***(2), pp. 255–267.

[20] Pan, G., and Meng, H., 2003. "Digital holography of particle fields: Reconstruction by use of complex amplitude". *Appl. Opt.,* ***42***(5), pp. 827–833.

[21] Yang, W., Kostinski, A. B., and Shaw, R. A., 2006. "Phase signature for particle detection with digital in-line holography". *Opt. Lett.,* ***31***(10), pp. 1399–1401.

[22] Dubois, F., Schockaert, C., Callens, N., and Yourassowsky, C., 2006. "Focus plane detection criteria in digital holography microscopy by amplitude analysis". *Opt. Express,* ***14***(13), pp. 5895–5908.

[23] Guildenbecher, D. R., Gao, J., Reu, P. L., and Chen, J., 2012. "Digital holography reconstruction algorithms to estimate the morphology and depth of nonspherical absorbing particles". *Proc. SPIE,* ***8493***(849303).

[24] Goodman, J. W., 1996. *Introduction to Fourier Optics*. McGraw-Hill.

[25] Tenenbaum, J. M., 1970. "Accomodation in computer vision". PhD thesis, Stanford University, Stanford, California.